Nanotechnology **21** (2010) 185603 (7pp) doi:10.1088/0957-4484/21/18/185603

Inorganic–organic elastomer nanocomposites from integrated ellipsoidal silica-coated hematite nanoparticles as crosslinking agents

A Sánchez-Ferrer[1], M Reufer[2], R Mezzenga[1], P Schurtenberger[2] and H Dietsch[2]

[1] ETH Zurich, Institute of Food, Nutrition & Health, Food & Soft Materials Science Group, Schmelzbergstrasse 9, 8092 Zurich, Switzerland
[2] Adolphe Merkle Institute and Fribourg Center for Nanomaterials, University of Fribourg, Route de l'Ancienne Papeterie, PO Box 209, 1723 Marly 1, Switzerland

E-mail: herve.dietsch@unifr.ch

Received 14 January 2010, in final form 10 March 2010
Published 14 April 2010
Online at stacks.iop.org/Nano/21/185603

Abstract
We report on the synthesis of nanocomposites with integrated ellipsoidal silica-coated hematite (SCH) spindle type nanoparticles which can act as crosslinking agents within an elastomeric matrix. Influence of the surface chemistry of the hematite, leading either to dispersed particles or crosslinked particles to the elastomer matrix, was studied via swelling, scattering and microscopy experiments. It appeared that without surface modification the SCH particles aggregate and act as defects whereas the surface modified SCH particles increase the crosslinking density and thus reduce the swelling properties of the nanocomposite in good solvent conditions. For the first time, inorganic SCH particles can be easily dispersed into a polymer network avoiding aggregation and enhancing the properties of the resulting inorganic–organic elastomer nanocomposite (IOEN).

(Some figures in this article are in colour only in the electronic version)

1. Introduction

Magnetic inorganic–organic network nanocomposites are covalently crosslinked polymeric systems, which can be found either in swollen state (magnetic gels) or in dry state (magnetic thermoplastics, thermosets or elastomers), and exhibit magnetic nanoparticles dispersed into the polymer matrix [1]. These materials have the combined advantages of organic polymers (flexibility and processability) and the inorganic nanoparticles (magnetic, optical and electrical properties) [2]. In this way, they can elongate and contract under magnetic field gradients and behave as soft actuators [3]. The concentration of magnetite nanoparticles and the crosslinking density play an essential and important role in their magneto-elastic behavior. These nanocomposites can be formed by the precipitation of magnetic nanoparticles in the organic material before, during, or after the crosslinking process [4, 5].

Several approaches have been reported for the integration of magnetic nanoparticles in a polymer network, including magnetic–polymer hydrogel nanocomposites [6, 7], magnetic–silica gel nanocomposites [8, 9], magnetic–latex nanocomposites [10], magnetic elastomer nanocomposites [11–13], magnetic–liquid-crystalline elastomer nanocomposites [14], and magnetic-shape memory polymer network nanocomposites [15].

Besides the dispersion of magnetic nanoparticles into a network, some attempts have been performed to covalently integrate magnetic nanoparticles into a polymer matrix in order to avoid their aggregation and the migration of the particles on application of external magnetic fields [16]. As a consequence, if the particles are directly attached to the polymer backbone of the gel network, a cooperative motion of the polymer network and the nanoparticles has to be expected. So far, a few examples can be found in literature where the nanoparticles

were used as physical crosslinkers in elastomers by means of supramolecular chemistry [17, 18], but no reports are found in which nanoparticles are used as covalent crosslinking agent.

The potential of such materials strongly depends on the coupling of both magnetic and elastic behavior. It is expected for hybrid nanocomposites with crosslinkable magnetic nanoparticles, that the application of an external magnetic field will affect the orientation of the particles; it can ultimately cause a change in the dimensions of the sample. Another expected effect will appear on applying unidirectional deformations to the sample, which should induce a rotation of the nanoparticles, and consequently a change in the magnetic response. Thus, this kind of hybrid nanocomposite can either work as actuators (when applying external magnetic fields), or as energy generators (when stretching–compressing them).

We describe here an *in situ* procedure for the integration of surface modified hematite nanoparticles that can act as covalent crosslinkers in the final elastomeric network. This reaction will be carried out during the gel network formation, ending up in a magnetic elastomer after removal of the solvent, due to the low glass transition temperature of the polymer chain selected. Our method consists of mixing the solution of nanoparticles, polymer chains and crosslinkers, the subsequent formation of a gel network after the crosslinking process, and finally obtaining inorganic–organic elastomer nanocomposites (IOENs). In more detail, we report for the first time the use of silica-coated hematite (SCH) nanoparticles as crosslinkers and the analysis of their hybrid nanocomposite properties. We compare this system with systems with non-crosslinkable nanoparticles, and with pure elastomeric networks made of the same polymer backbones.

2. Experimental details

2.1. Materials

Iron (III) perchlorate hexahydrate ($Fe(ClO_4)_3{\cdot}6H_2O$), poly (vinylpyrrolidone) (PVP, 10 000 g mol^{-1}), tetramethylammonium hydroxide (TMAH) 25% solution in methanol were all provided by Sigma Aldrich and used as received. Sodium dihydrogen phosphate monohydrate ($NaH_2PO_4{\cdot}H_2O$), urea and absolute ethanol from Fluka, tetraethyl orthosilicate (TEOS) and acetone from Merck, 3-aminopropyltriethoxysilane (APTES) from ABCR were also used without further purification. Ultrapure water (18.2 MΩ cm) purified by a MilliQ system, was used throughout the experiments.

The diamine-terminated poly(propylene oxide) polymer Jeffamine® D-2000 with approximate number average molecular mass of M_n = 2000 g mol^{-1} was kindly provided by Huntsman Corporation and degassed before use. The triisocyanate crosslinker Basonat® HI-100 was kindly provided by BASF SE and used as received.

2.2. Synthesis of functional ellipsoidal silica-coated hematite nanoparticles

Spindle type hematite nanoparticles were synthesized according to the method previously described [19]. In a typical synthesis, an aqueous solution of iron (III) perchlorate (100 mM), sodium phosphate monobasic (5.5 mM) and urea (100 mM) was kept in an oven at 98 °C for 24 h. The precipitated particles were then washed five times by centrifugation at 10 000 rpm for 15 min followed by redispersion in water using an ultrasonic bath.

Based on a previous work [20], 150 mg of particles were dispersed in a solution of PVP (M_w = 40 000 g mol^{-1}). The amount of PVP was calculated to have about 13 PVP molecules per square nanometer of particle surface. The suspension was stirred for 12 h to let the polymer adsorb onto the surface. The stabilized particles were then transferred in 485 ml of a mixture of water (17.5%), absolute ethanol (82.5%) and tetramethylammonium (0.015%, 25% solution in methanol). While stirring and sonicating, a 1:2 mixture of TEOS (99.0%) and ethanol was added in three shots of 6 ml each every 20 min. Finally, 30 min after the last TEOS addition, 160 μl of APTES was added (for non-surface functionalized nanoparticles, APTES was not used). Sonication was applied for 2 h after the last injection and the mechanical stirring was further continued overnight at room temperature. The particles were then washed by centrifugation and redispersion.

After adding acetone to the aqueous nanoparticle dispersion, the precipitate was washed five times by centrifugation at 10 000 rpm for 15 min, followed by redispersion in acetone using an ultrasonic bath. The final concentrations of amino-functionalized SCH nanoparticles and normal SCH nanoparticles were 1.4 mg ml^{-1} and 2.8 mg ml^{-1} respectively.

2.3. Synthesis of the inorganic–organic elastomer nanocomposites

Three elastomers were synthesized: a reference elastomer (E0) without any nanoparticle, and two elastomers containing SCH nanoparticles. The two SCH nanoparticles in the matrix were either functionalized with amino groups on the surface of the silica-coated hematite (E1), or bare silica-coated hematite nanoparticles (E2). For the synthesis of the three elastomers, two solutions in acetone were prepared: one containing the diamino-terminated polymer, and the other the tri-functionalized crosslinker with or without nanoparticles.

In order to obtain a final solid content of 15 w/v%, 3.85 g of Jeffamine® D-2000 was dissolved in 11.1 ml of acetone in one 50 ml plastic flask, and 0.65 g of Basonat® HI-100 were dissolved in 14.5 ml of acetone in a second 50 ml plastic flask. In the case of elastomers containing SCH nanoparticles, the Basonat® HI-100 was dissolved in an acetone dispersion of the corresponding nanoparticles to be incorporated (150–275 mg of nanoparticles in 100 ml of acetone). The two solutions were mixed and gently stirred for 5 min, and the final solution was cast onto the glass surface of a Petri dish. One day after the sample was cast, the obtained film was allowed to dry in the atmosphere, and peeled from the surface [21].

2.4. Methods

A Leica DM LB optical microscope equipped with a Linkam CSS450 hot-stage was used to analyze the homogeneity of the samples.

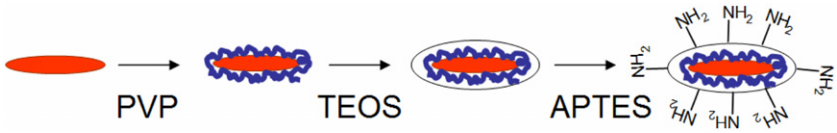

Scheme 1. Poly(vinylpyrrolidone) (PVP) adsorption, silica coating and surface modification of the spindle hematite nanoparticles.

Fourier transform infrared (FTIR) spectra of the solid samples were recorded at room temperature with a Bruker Tensor 27 FTIR spectrometer and using a MKII golden gate single attenuated total reflection (ATR) system.

Transmission electron microscopy (TEM) images were obtained with a Philips TEM (CM 100) instrument operated at 80 kV. The elastomeric samples were cryo-ultramicrotomed at −80 °C using a diamond knife on a Leica Ultracut UCT Ultramicrotome to give 50 nm thick sections. Sections were then transferred onto 600-mesh carbon-coated copper grids. Nanoparticles were visualized by concentrating the particle dispersions using a lab centrifuge at 10 000 rpm, and drying one droplet of 1 vol% of particles onto a 300-mesh carbon-coated copper grid.

Simultaneous small and wide angle x-ray scattering (SWAXS) measurements and small angle x-ray scattering (SAXS) measurements were performed using Anton-Paar SAXS's and Rigaku diffractometers in order to obtain direct information on the low and high scattering vector ranges, respectively.

Thermal gravimetric analysis (TGA) experiments were performed using a TGA/SDTA851e apparatus from Mettler Toledo equipped with an autosampler TS0801R0, and 70 μl aluminum oxide crucibles. Measurements were performed at a temperature rate of 5 °C min^{-1} from 60 °C up to 700 °C with an air flow of 300 ml min^{-1}.

Swelling experiments were performed in acetone at 25 °C, to obtain information on the effective crosslinking density as compared to other elastomers. The sizes of the dry and swollen elastomer sample were determined using a Will Strübin–Wetzlar optical microscope. The swelling parameter ($Q = \alpha^3$) is the ratio of the volumes of the swollen to dry elastomer, where Q is the isotropic linear swelling parameter.

3. Results and discussion

3.1. Synthesis of inorganic–organic elastomer nanocomposites

Inorganic–organic elastomer nanocomposites (IOENs) can be obtained by integrating surface-functionalized nanoparticles which take part during the crosslinking of the gel network. We have already described this *in situ* procedure in the past by integrating surface modified silica particles within a poly(methylmethacrylate) matrix which was afterward attached to the polymer backbone via UV radical polymerization process [22]. We propose here the integration of SCH nanoparticles for their ability to orient under a magnetic field on their short axis [23]. In order to allow such an integration, we further coat the nanoparticles with a silica layer according to the general method described by Graf *et al* [24]. Scheme 1 presents this coating procedure followed by a surface modification using a silane coupling agent (3-aminopropyltriethoxysilane, APTES) which is used for various purposes such as binding a fluorescent marker [20], enzyme or simply changing the surface charges at the same pH conditions.

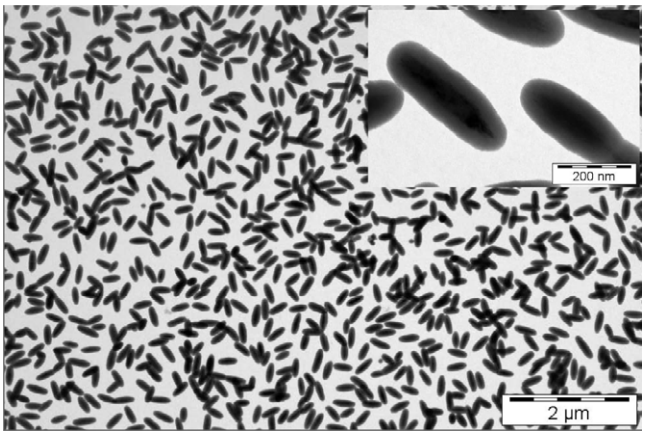

Figure 1. TEM images of core–shell ellipsoidal SCH nanoparticles. The higher magnification image in the inset better captures the contrast between the hematite core and the silica shell.

Figure 1 shows transmission electron microscope (TEM) micrographs of the ellipsoidal SCH particles. After the synthesis of the core–shell inorganic ellipsoidal particles, one can envisage integrating them during the elastomer polymerization step and so replacing the crosslinking agent generally used in classical crosslinking processes. The amino groups then decorating the surface of the SCH nanoparticles take part in the synthesis by reacting with the isocyanate groups from the crosslinker. They act as chain extenders and connectors to the polymer chains, which also have amino-terminated groups.

The two IOENs (E1 and E2) and the reference elastomer (E0) were synthesized by condensation of the amino groups from the polymer chains (Jeffamine® D-2000) and the isocyanate groups from the crosslinker (Basonat® HI-100), leading to the corresponding formation of urea groups, and the elastomeric matrix. The SCH nanoparticles that were surface modified with amino groups also had the ability to act as multifunctionalized crosslinkers, increasing the local crosslinking density in their IOEN (E1). On the contrary, the SCH nanoparticles that were not functionalized remained dispersed in the elastomeric network (E2). In fact, this second IOEN sample (E2) should have the swelling properties of a simple reference elastomer where the nanoparticles could be integrated by a solvent process.

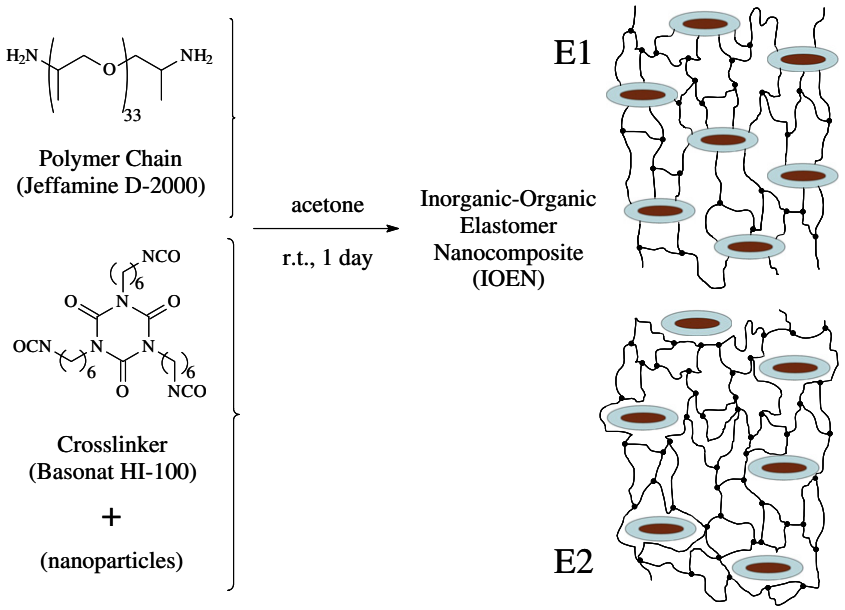

Scheme 2. Chemical structures of the organic components for the synthesis of IOENs, and their corresponding topology as function of the reactive (E1) or non-reactive (E2) particles.

In scheme 2, the chemical structures and the final topology of both IOEN classes are depicted. One should expect some noticeable differences between the two systems since the nanoparticles play a different role in the two classes of hybrid IOEN materials (e.g. fillers versus crosslinkers). In other words, the sample with reactive nanoparticles (E1) should present a higher degree of crosslinking than the sample with non-reactive nanoparticles (E2). This difference in the degree of crosslinking is expected to be reflected by the mechanical, thermal and optical properties of the sample with respect to both the normal reference system and the dispersed nanoparticle system.

3.2. Characterization of inorganic–organic elastomer nanocomposites

In order to analyze both systems with or without crosslinkable SCH particles, some experiments were carried out to observe differences in the thermal, optical and mechanical behavior.

Thermal behavior of the three elastomers was also studied in order to analyze the effect of the presence of SCH nanoparticles in the network and their reactivity with the organic matrix. Figure 2 is the plot of the three thermograms of the studied systems in the presence of air. From the curves, it can be observed that the sample with non-crosslinkable nanoparticles behaves almost equally to the reference system. The presence of the free nanoparticles inside the matrix does not affect the polymer network, which appears to behave independently. All samples start to decompose almost at the same temperature, but the elastomer with crosslinkable nanoparticles has a delay of its inflection point—maximum loss during oxidation—of 25 °C (at 333 °C) from the analysis of their derivatives. It seems that the crosslinkable nanoparticles reinforce the elastomer and at the same time thermally stabilize it.

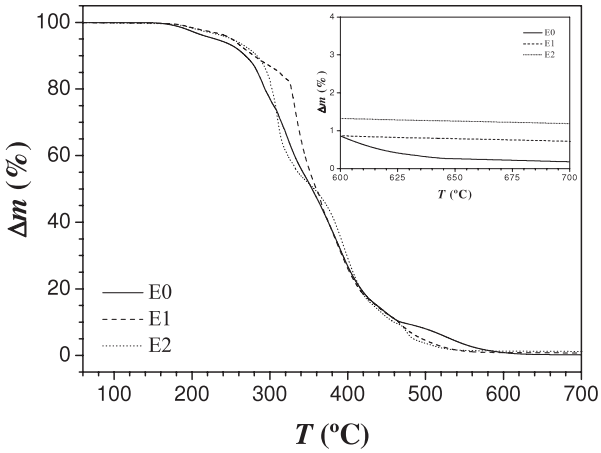

Figure 2. TGA thermograms of the two IOENs (E1 and E2) and the reference sample (E0). The inset is the final value after total oxidation of the samples.

The residual mass after the experiments was 0.72% for the sample E1, 1.12% for the sample E2, and 0.18% for the sample E0. These results are in agreement with the quantities employed for the synthesis of both IOENs of 0.46% (E1) and 0.89% (E2).

Optical microscopy experiments already reveal large differences in the degree of homogeneity between the two samples (figure 3). The sample with crosslinkable nanoparticles (E1) shows a reddish color and few defects through the section. The other sample with nanoparticles dispersed in the network (E2) shows the presence of large aggregates within the entire section and strong heterogeneities.

The degree of crosslinking is a parameter that is related to the mechanical properties and swelling of the networks. The swelling process is the equilibrium between the two driving

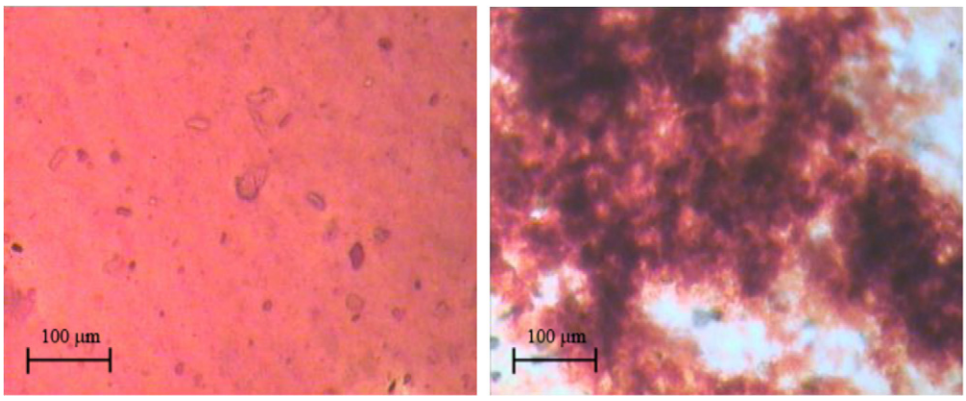

Figure 3. Optical microscopy images of the IOEN with functionalized SCH nanoparticles (E1, left) and IOEN with non-functionalized SCH nanoparticles (E2, right).

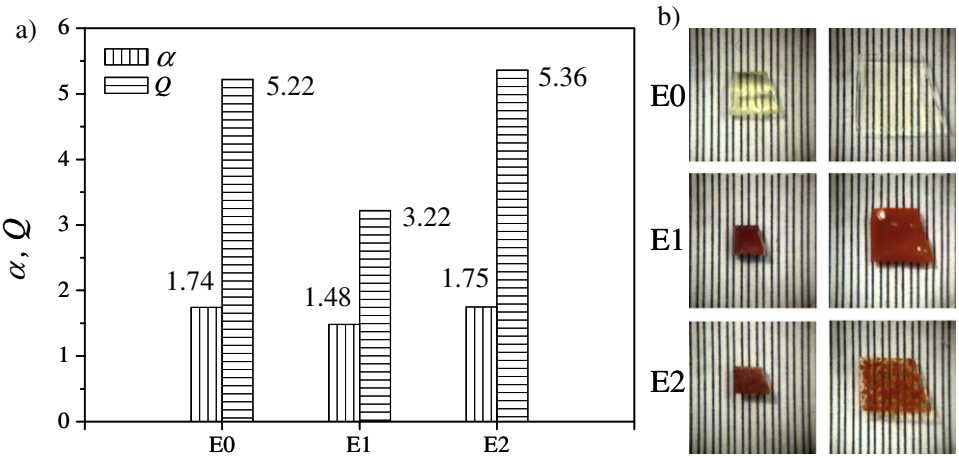

Figure 4. (a) Linear swelling parameter (α) and volumetric swelling parameter (Q) for the two elastomeric samples (E0, E1 and E2). (b) Pictures of the unswollen and swollen dimensions for the three networks at 25 °C.

forces involved, where the solvent molecules tend to solvate the polymer chains of the network (mixing) and the retractive elastic force of chains tends to maintained their original unstretched maximal entropy conformation (elasticity). Thus, samples that show a higher degree of crosslinking should present a lower degree of swelling, and vice versa. In figure 4, the isotropic linear swelling parameter (α) and the volumetric swelling parameter (Q) are represented for all the samples, including the reference elastomer without any nanoparticles.

From these results, it can be concluded that the IOEN E2 has a swelling parameter of $Q = 5.36$, nearly identical to that of the reference elastomer E0 of $Q = 5.22$. The small difference can be explained by the defects introduced into the network by the presence of the nanoparticles, which impede the full crosslinking process. On the contrary, the IOEN E1 shows a lower swelling parameter of $Q = 3.22$, which can be explained by means of higher crosslinking density around the nanoparticles, while maintaining constant the length of the polymer chain.

Small and wide angle x-ray scattering (SWAXS) experiments were also performed to study the distribution of the nanoparticles in the polymer network matrix. In figure 5(a), the SWAXS diffractograms of the three samples are shown. The first noticeable fact is that the two IOENs (E1 and E2) scatter much more than the reference elastomer (E0) at low q values. This is indeed a signature of the presence of these inorganic nanoparticles, which have dimensions much larger (100–200 nm) than the polymer chains (1–5 nm).

The two broad peaks at $q = 14.4$ nm^{-1} ($d = 0.44$ nm) and at $q = 1.20$ nm^{-1} ($d = 5.2$ nm) represent the distance between the polypropylene oxide chains, and the disordered micro-phase separated domains between the aliphatic segments of the crosslinker and the ether segments of the polymer chains, respectively. This phase separation is enhanced by the presence of hydrogen bonding of the urea motifs appearing during the condensation polymerization process.

To reveal more information on the embedding of the SCH in the IOENs we fit the low q-region of the scattering data with a model based on a form factor of a core–shell ellipsoid, where the core accounts for the SCH and the shell describes the polymer layer modified by the presence of the SCH. The used model is described in more detail in the literature, including an application on similar particles [25]. Figure 5(b) shows the data with the fits obtained, and in the inset the core–shell particle model used for the fits is reproduced. The best-fit parameters for the semi-axis of the SCH are $a = 129$ nm

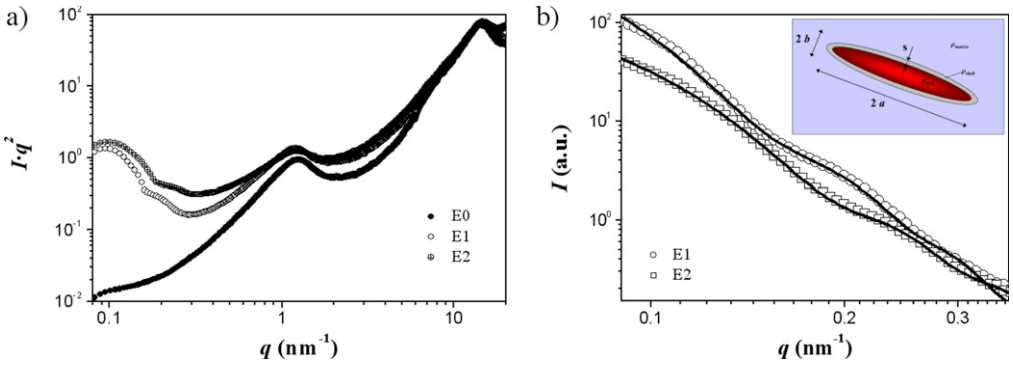

Figure 5. (a) SWAXS diffractograms of the two IOENs (E1 and E2) and the reference elastomer (E0) at 25 °C. (b) Close up of the low q-region with the fitted curves for E1 and E2. The inset shows a core–shell particle as used in the model for the fits.

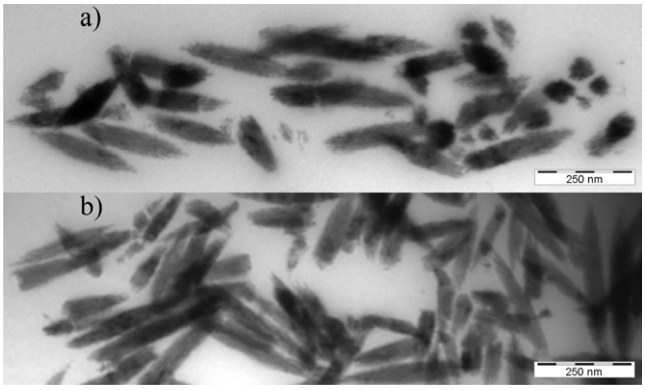

Figure 6. TEM images of (a) the IOEN (E1) with crosslinkable hematite silica core–shell ellipsoidal nanoparticles and of (b) the IOEN (E2) with the non-crosslinkable nanoparticles.

for E1 (114 nm for E2) and $b = 26$ nm (23 nm) with a polydispersity of 0.5 and a shell thickness of 4.8 nm (4.2 nm) with polydispersity of 0.2. The slightly larger size particle size of the E1 particle might be attributed to the additional surface modification of the SCH particles. However, the most remarkable results are the scattering contrasts found for the shell. Whereas the scattering length density for the hematite particle and the polymer matrix were kept at $\rho_{\text{hem}} = 4.10 \times 10^{-3}$ nm^{-2} and $\rho_{\text{matrix}} = 0.97 \times 10^{-3}$ nm^{-2}, respectively, we used the scattering length density for the particles shell ρ_{shell}(Ex) as a fitting parameter and found ρ_{shell}(E1) $= 2.10 \times 10^{-3}$ nm^{-2} for E1 and ρ_{shell}(E2) $= 0.23 \times 10^{-3}$ nm^{-2} for E2. The values found correspond to relative polymer densities for the shell around the SCH in E1 of 2.3 and in E2 of 0.24. This suggests that the higher local crosslinking in the vicinity of the reactive particles E1 leads to an increased polymer density, whereas the non-reactive particles E2 show a locally lowered polymer density due to the incompatible coating.

TEM experiments were also performed to obtain information about the local aggregation of the SCH nanoparticles in the elastomeric matrix. In figure 6, the two samples are shown from images acquired on 50 nm thick sections. It can be observed that the sample containing non-crosslinkable SCH nanoparticles (E2) shows a higher tendency for aggregation, while for the crosslinkable SCH containing nanoparticles (E1) better dispersion was obtained.

A controlled integration in terms of dispersion and distribution within the nanocomposite can be claimed for the sample E1. This demonstrates that modifying the surface functionality such that the particle surfaces take part in the polymerization process provides a suitable technique to alter the swelling properties of elastomers. The use of such magnetic nanocomposite elastomers does of course critically depend upon the magnetic properties of the integrated nanoparticles. Hematite particles are so-called canted antiferromagnets above the Morin temperature (250 K) and below the Néel temperature (1000 K), therefore they have a very small remanent magnetic moment (0.02 emu g^{-1} [26]), low magnetic susceptibility and low saturation magnetization, and are thus not suited for applications as actuators. The magnetic susceptibility of the hematite particles is in fact sufficiently large to achieve a significant alignment in aqueous dispersion [25] or prior to *in situ* polymerization. However, alignment of the hematite particles within the elastomeric matrix could be achieved neither after the polymerization nor in the swollen state of the nanocomposite E1.

An alternative could be maghemite particles, which can easily be obtained with the same morphology through a transformation from hematite [27]. These particles would then become ferromagnetic with a remanent moment about 200 times larger than that of hematite. However, while a strong magnetic moment of the particles is essential for many applications, a remanent moment that is also present in the absence of an external magnetic field during the synthesis would induce a significant magnetic attraction between the particles and thus limit our ability to integrate them without aggregation. Magnetite would on the other hand be ideal, as these particles have a high susceptibility and no remanent moment (superparamagnetic behavior); however, available particle morphologies are currently limited to isotropic single domain particles, which are clearly not ideal for actuation. It is for these reasons that we are currently working on new synthesis schemes to combine an anisotropic particle shape with high susceptibility and superparamagnetic-like low remanent moments.

4. Conclusions

Two inorganic–organic elastomer nanocomposites (IOENs) have been synthesized by using two different silica-coated

hematite (SCH) particles, a diamino-terminated poly(propylene oxide) polymer chain and a triisocyanate based crosslinker. In one case the particles were surface modified by attaching amino-functionalized groups on the surface of the silica layer, and in the second case the particles were kept bare without any further modification. These amino groups are suitable for condensation with isocyanate functional groups, and the same chemistry as the ending groups of the polymer chains was used, allowing the formation of elastomer films by urea linkage.

The introduction of the crosslinkable SCH particles strongly modifies the properties of the hybrid composite, which is reflected in the swelling, scattering and thermal behavior. We obtained a good dispersion of the particles in the polymer matrix with no apparent aggregation. The SCH particles enhance the local crosslinking density, as confirmed by the SAXS experiment, and thus lead to the observed reduced swelling behavior.

For the first time, inorganic nanoparticles have been successfully dispersed in a polymer network by covalent bond linkage. This approach is of great interest due to the modification of the final material properties with respect to the homogeneous organic polymeric system, and can thus bypass the use in nanocomposite materials of large quantities of the common non-modified nanoparticles or fillers.

Acknowledgments

The authors would like to acknowledge the financial support provided by the Adolphe Merkle Foundation, the Swiss National Science Foundation (project No. 200020-117755), and the State Secretariat for Education and Research and COST Action D43. Benoît Droz is thanked for his help with the TGA measurements.

References

[1] Zrínyi M 1997 *Trends Polym. Sci.* **5** 280–5
[2] Althues H, Henle J and Kaskel S 2007 *Chem. Soc. Rev.* **36** 1454–65
[3] Zrínyi M, Barsi L and Büki A 1997 *Polym. Gels Netw.* **5** 415–27
[4] Zrínyi M, Barsi L, Szabó D and Kilian H G 1997 *J. Chem. Phys.* **106** 5685–93
[5] Mitsumata T, Ikeda K, Gong J P, Osada Y, Szabó D and Zrínyi M 1999 *J. Appl. Phys.* **85** 8451–6
[6] Zrínyi M, Barsi L and Büki A 1996 *J. Chem. Phys.* **104** 8750–6
[7] Collin D, Auernhammer G K, Gavat O, Martinoty P and Brand H R 2003 *Macromol. Rapid Commun.* **24** 737–41
[8] Bentivegna F *et al* 1998 *J. Appl. Phys.* **83** 7776–88
[9] Bentivegna F, Nyvlt M, Ferré J, Jamet J P, Brun A, Višňovsky Š and Urban R 1999 *J. Appl. Phys.* **85** 2270–8
[10] Lee C F, Chou Y H and Chiu W Y 2007 *J. Polym. Sci.* A **45** 3062–72
[11] Sena C, Godinho M H and Figueiredo Neto A M 2007 *J. Appl. Phys.* **102** 073524
[12] Figueiredo Neto A M, Godinho M H, Toth-Katona T and Palffy-Muhoray P 2005 *Braz. J. Phys.* **35** 184–9
[13] Ghosh A, Sheridon N K and Fischer P 2008 *Small* **4** 1956–8
[14] Kaiser A, Winkler M, Krause S, Finkelmann H and Schmidt A M 2009 *J. Mater. Chem.* **19** 538–43
[15] Schmidt A M 2006 *Macromol. Rapid Commun.* **27** 1168–72
[16] Fuhrer R, Athanassiou E K, Luechinger N A and Stark W J 2009 *Small* **5** 383–8
[17] Song H M, Kim J C, Hong J H, Lee Y B, Choi J, Lee J I, Kim W S, Kim J H and Hur N H 2007 *Adv. Funct. Mater.* **17** 2070–6
[18] Song H M, Kim Y J and Park J H 2008 *J. Phys. Chem.* C **112** 5397–404
[19] Ocaña M, Morales M P and Serna C J 1999 *J. Colloid Interface Sci.* **212** 317–23
[20] Sacanna S, Rossi L, Kuipers B and Philipse A 2006 *Langmuir* **22** 1822–7
[21] Sánchez-Ferrer A, Rogez D and Martinoty P 2010 *Macromol. Chem. Phys.* submitted
[22] Saric M, Dietsch H and Schurtenberger P 2006 *Colloids Surf.* A **291** 110–6
[23] Reufer M, Dietsch H, Gasser U, Grobety B, Malik V K, Hirt A and Schurtenberger P 2010 in preparation
[24] Graf C, Vossen D L, Imhof A and Blaaderen A 2003 *Langmuir* **19** 6693–700
[25] Reufer M, Dietsch H, Gasser U, Hirt A, Menzel A and Schurtenberger P 2010 *J. Phys. Chem.* B doi:10.1021/jp911817e
[26] Dietsch H *et al* 2008 *Chimia* **62** 805–14
[27] Ozaki M and Matijevic E 1985 *J. Colloid Interface Sci.* **107** 199–203